air

MDPI

Article

Nontrivial Impact of Relative Humidity on Organic New Particle Formation from Ozonolysis of *cis*-3-Hexenyl Acetate

Austin C. Flueckiger †, Christopher N. Snyder † and Giuseppe A. Petrucci *

Department of Chemistry, The University of Vermont, 82 University Place, Burlington, VT 05405, USA; afluecki@uvm.edu (A.C.F.); cnsnyder@uvm.edu (C.N.S.)

* Correspondence: giuseppe.petrucci@uvm.edu

† These authors contributed equally to this work.

Abstract: The impact of relative humidity (RH) on organic new particle formation (NPF) from the ozonolysis of biogenic volatile organic compounds (BVOCs) remains an area of active debate. Previous reports provide contradictory results, indicating both the depression and enhancement of NPF under conditions of high RH. Herein, we report on the impact of RH on NPF from the dark ozonolysis of *cis*-3-hexenyl acetate (CHA), a green-leaf volatile (GLV) emitted by vegetation. We show that RH inhibits NPF by this BVOC, essentially shutting it down at RH levels > 1%. While the mechanism for the inhibition of NPF remains unclear, we demonstrate that it is likely not due to increased losses of CHA to the humid chamber walls. New oxidation products dominant under humid conditions are proposed that, based on estimated vapor pressures (VPs), should enhance NPF; however, it is possible that the vapor phase concentration of these low-volatility products is not sufficient to initiate NPF. Furthermore, the reaction of C_3-excited state Criegee intermediates (CIs) with water may lead to the formation of small carboxylic acids that do not contribute to NPF. This hypothesis is supported by experiments with quaternary O_3 + CHA + α-pinene + RH systems, which showed decreases in total α-pinene-derived NPF at ~0% RH and subsequent recovery at elevated RH.

Keywords: CHA; secondary organic aerosol; SOA; aerosol mass spectrometry; green-leaf volatile; GLV

Citation: Flueckiger, A.C.; Snyder, C.N.; Petrucci, G.A. Nontrivial Impact of Relative Humidity on Organic New Particle Formation from Ozonolysis of *cis*-3-Hexenyl Acetate. *Air* **2023**, *1*, 222–236. https://doi.org/10.3390/air1040017

Academic Editor: Ling Tim Wong

Received: 3 August 2023
Revised: 6 October 2023
Accepted: 13 October 2023
Published: 17 October 2023

1. Introduction

Volatile organic compounds in the atmosphere contribute significantly to secondary organic aerosol (SOA) [1,2]. Some estimates place the fraction of SOA mass in fine and ultrafine particles in continental air masses to be greater than 70% [1,3,4]. Biogenic volatile organic compounds (BVOCs), such as monoterpenes and green-leaf volatiles (GLVs), are major contributors to atmospheric SOA by way of oxidation with atmospheric gases to form low-volatility compounds that either form new particles or partition to existing particles [5–13]. *Cis*-3-hexenyl acetate (CHA) is one of several stress-induced GLVs emitted by green-leaf plants that has been shown to generate SOA in laboratory studies [14] and could be a significant contributor to the SOA mass in regional airsheds [15–18]. To date, however, all studies to the authors' knowledge have considered only SOA mass formation (C_{SOA}) under dry conditions, and no studies have been undertaken on the impact of atmospherically relevant relative humidities (RHs) on new particle formation (NPF) from this GLV. Similarly, the vast majority of studies to date on NPF and C_{SOA} from the dark ozonolysis of monoterpenes have been conducted at fixed and uncharacteristically low levels of RH that are not representative of the lower troposphere [19], which is where most of the NPF and C_{SOA} are hypothesized to occur [9,20–25]. Recently, studies have been reported to better understand the role of RH in NPF and SOA generation from the ozonolysis of several monoterpenes, including α- and β-pinene [26–31], limonene [27,28], and ^{3}Δ-carene [27,28]. Reported results have been contradictory, with some reporting an enhancement in NPF and C_{SOA} as a result of higher RH [27,31–33], while others report

sharp decreases [28,31,34–38]. The cause(s) of these discrepancies remains unclear. Further exacerbating the issue are the different VOCs and oxidant mixing ratios (ξ_{VOC} and ξ_{O3}) used in laboratory studies, which have ranged from parts-per-trillion by volume ($pptr_v$) to parts-per-million by volume (ppm_v), the latter predominantly in studies employing flow reactors with reaction times of up to a few minutes only. It is unlikely that results obtained at these high ξ_{VOC}/ξ_{O3} are representative of the natural environment, thereby providing inaccurate data and guidance to atmospheric modelling efforts. For example, recently, we reported on significant enhancements in NPF for the dark ozonolysis of α- and β-pinene at $\xi_{VOC} < 20$ ppb_v in the presence of high RH [26].

Herein, we report on laboratory environmental chamber studies on the impact of RH on NPF and C_{SOA} in both ternary (CHA + O_3 + RH) and quaternary (CHA + α-pinene + O_3 + RH) systems. Systematic experiments at varying ξ_{VOCs} and RHs were carried out to gain an improved understanding of the quantitative nature of the RH impact, as well as potential mechanisms likely producing the observed outcomes. A scanning mobility particle sizer (SMPS) was used to quantify NPF and infer C_{SOA}. An electrical low-pressure impactor (ELPI+) was used to determine time-evolution particle and size distributions. Soft ionization near-infrared aerosol mass spectrometry was used for the chemical analysis of the SOA at mass loadings as low as 1 μg m^{-3}. We show that RH impacts NPF in a nonlinear manner and that the correlation of NPF with RH could be positive or negative as a function of the chemical system and ξ_{VOC}.

2. Materials and Methods

2.1. Reagents

CHA (>97.0%) was purchased from TCI (Portland, OR, USA) and (+)-α-pinene (98%) was purchased from Alfa Aesar (Haverhill, MA, USA). Both were used without further purification. In all experiments, ozone was produced using a commercial generator (OL80A/DLS, Ozone Lab, Burton, BC, Canada) using dry, particle-free (zero) air. Ozone was injected by diverting the output flow of the generator to the chamber for a pre-determined time pulse to yield the desired ozone concentration. Typical injection pulses were in the range of 10–120 s, depending on the size of the chamber in use.

2.2. Experimental Conditions and Instrumentation

All experiments were conducted under ambient temperature and atmospheric pressure. Two Teflon reaction chambers were utilized separately for this work and are referred to as the 775 L particle genesis chamber (PGC) and the 8 m^3 University of Vermont Environmental Chamber (UVMEC) [39]. For both types of reaction chambers, zero air was used for flushing (after H_2O_2 passivation with UV lamps) until the background aerosol mass and number concentrations were below 0.01 μg m^{-3} and 10 particles cm^{-3}, respectively.

Aerosol particle size distributions were measured using a scanning mobility particle sizer (SMPS 3082, TSI Inc., Shoreview, MN, USA) operating with sheath and aerosol flows of 3 and 0.3 L min^{-1}, respectively. C_{SOA} was estimated by assuming spherical particles with a density of 1.3 g cm^{-3}, in accord with the predictive estimates of Nakao et al. [40]. Aerosol particle size distributions were also measured using an electrical low-pressure impactor (ELPI+, Dekati Technologies Ltd., Kangasala, Finland), where particles were sorted into 14 different size-bins at s^{-1}. The ELPI+ provides much higher temporal resolution (1 Hz scan rate) than the SMPS, allowing for time-evolution measurements of the SOA, albeit at lower size resolution. Chemical analysis of the SOA was carried out using a custom-built Near-Infrared Laser Desorption/Ionization Aerosol Mass Spectrometer (NIR-LDI-AMS) [39,41]. Aerosol sampling occurred through a Liu-type aerodynamic lens, and the SOA was collimated into a particle beam that was aligned to deposit aerosol mass onto the tip of a 1 mm diameter aluminum probe (99.9% purity, ESPI metals, Ashland, OR, USA) suspended under high vacuum in the ionization region of the mass spectrometer. Particles collected on the probe's tip were both desorbed and ionized using a single pulse from an unfocused, 3 mm diameter Nd:YAG laser (Brio, Quantel USA, Big Sky, CO) with a 20 mJ,

4 ns half-width pulse. The deposited SOA mass was entirely desorbed by 2–3 laser shots. A time-of-flight mass analyzer was used for ion detection with a working mass range from 0 to 500 m/z and a mass resolution of 1000 at 300 m/z. For each experiment, mass spectra were collected at 0.1–2 min intervals over the course of approximately 60 min.

2.3. General Methodology

C_{SOA} values obtained from SMPS measurements have been corrected for wall losses using ammonium sulfate reference aerosol in accordance with a previously established method [42]. Standard deviations are estimated based on a previous report that systematically evaluated instrumental errors in our chamber measurements [43]. In accord with this previously established method [43], ξ_{O3} was established in the chamber prior to injection of the VOC, which helped minimize variability in the measurements. It may be that the order in which the reagents are injected will impact the outcomes; however, this is beyond the scope of the present study. In all experiments, ξ_{VOC} and ξ_{O3} were 100–270 ($\pm$10) and 200–500 ($\pm$20) ppb_v, respectively, depending on the specific experiment (detailed in each table/figure). The temperature inside the chamber, while not actively controlled, was 22 ($\pm$1) °C. Once the RH and ξ_{O3} were established and equilibrated in the chamber (10–15 min after O_3 injection), a glass micro-syringe (Hamilton 7000 series gas-tight syringe) was used to quantitatively transfer VOC aliquots to a glass three-neck flask that was placed in a hot water bath (80 $\pm$ 2 °C). For the ternary system experiments, a split valve and stop/flow valve were used on the injection line with a 2 L min^{-1} flow of zero air to the UVMEC to permit particle measurements at low ξ_{VOC} (detailed here: [43]). For the quaternary system experiments, a solution mixture of CHA and α-pinene was prepared (dissolving α-pinene directly into CHA) to the desired mole ratio, permitting both VOCs to be injected as a single aliquot. The liquid-phase VOC content within the flask was visually monitored as a 6 L min^{-1} flow of zero air carried the volatilized VOC into the reaction chamber. Once all of the VOC was introduced, the zero air flow was shut off after 10–20 min of continuous flow. The mole ratio of CHA:α-pinene was 2:1 in all cases, which would result in a ratio of C5:C10-Criegee intermediates (CIs) at 2:1.

2.4. Humidification of the Chambers

For RHs exceeding ~2%, RH was established in the chamber by a tandem bottle setup, where a 6 L min^{-1} flow of zero air passed through a gently heated 4 L bottle containing 0.5 L of reverse osmosis water, then flowed through an additional 4 L bottle held at room temperature before entering the chamber (Figure 1a). For low RHs (<2%), RH was established in the chamber by quantitative transfer of a liquid water aliquot (high purity, reverse osmosis) via a 100 µL gas-tight glass syringe to a heated box setup (Figure 1b) through a rubber septum. This approach uses a three-neck U-shaped glass assembly housed in an aluminum box with an internal wax media; the apparatus sits on a hotplate to maintain a desired temperature (90 $\pm$ 2 °C). Zero air flowing at 2 L min^{-1} was used to transfer the vaporized water aliquot to the UVMEC. Each transfer of 100 µL equated to approximately 0.1% RH. Multiple transfers were used to attain the desired RH for a given experiment. RH and temperature in the chamber were measured using a Vaisala HUMICAP® HMT130 dual sensor (Vaisala Inc, Vantaa, Finland).

It is important to note that the recirculating sheath air in the SMPS remained at RH < 30% for the duration of any single experiment, so any liquid water taken up by organic particles in the reaction chamber should quickly evaporate during size measurement. We confirmed that SOA size distributions measured at high RH in the chamber were for dried particles by comparing particle size distributions pre- and post-passage through a 30 cm diffusion drier. No difference in size distribution was measured, *suggesting that the SOA particles measured with the SMPS are "fully dried", and that measured increases in particle number concentration (N), SOA mass (C_{SOA}), and geometric mean diameter (GMD) correspond only to particulate organic material*.

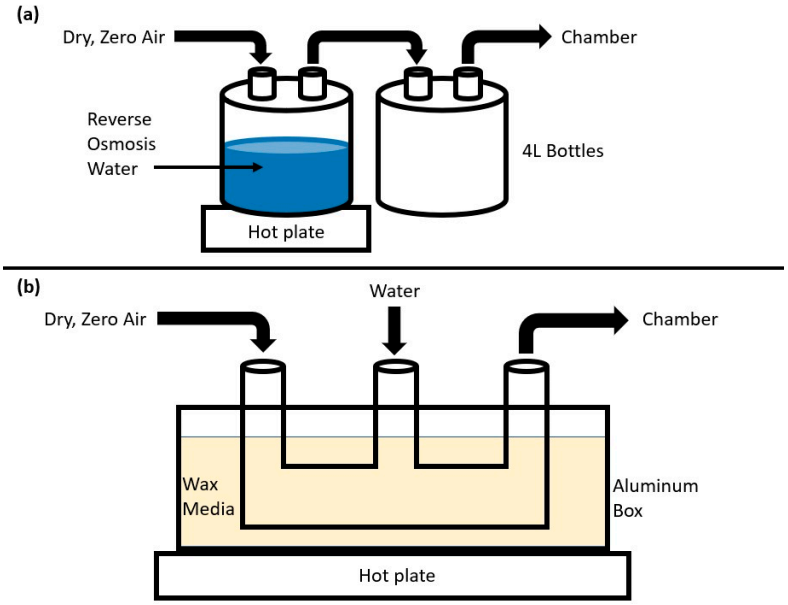

Figure 1. Humidity setup for (**a**) modest to high RHs (>2%) and (**b**) low RHs (<2%).

2.5. AMS Methodology

Chemical analysis of SOA particles was carried out by NIR-LDI-AMS. This approach, developed in the authors' laboratory, uses a low energy, near-infrared laser pulse to vaporize and ionize SOA particles with little to no molecular fragmentation, producing predominantly $[M\text{-}H]^-$ ions. This soft ionization approach produces simplified mass spectra, facilitating molecular analysis and providing chemical profiles of SOA particles. A detailed description of NIR-LDI-AMS for SOA chemical analysis is provided elsewhere [39,41].

Newly formed organic particles were sampled with a condensation and growth apparatus (CGA) developed in house (Figure 2) [44]. The CGA was optimized to utilize a squalane matrix to (1) prevent mass spectral interferences in the chemical analysis of the SOA and (2) grow all nascent particles with diameters greater than a few nm to a fixed diameter of 110 nm, ideal for aerodynamic sampling using a Liu-type lens. The authors are aware of only one other research group using a similar approach to sample and analyze water-soluble nanoparticles (NPs) [45].

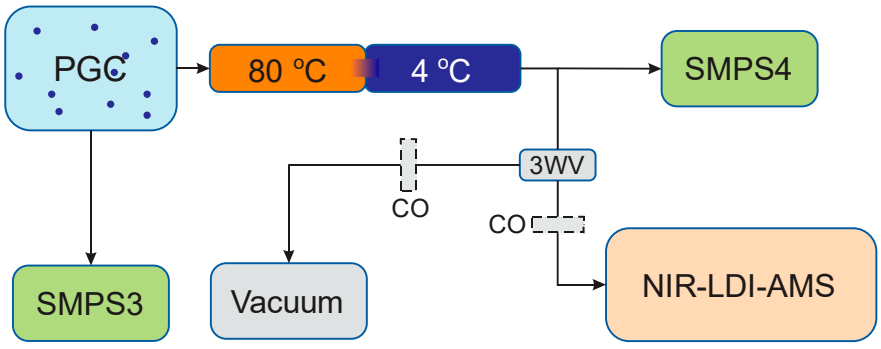

Figure 2. Experimental setup for CGA. 3WV = 3-way valve, CO = 150 µm critical orifice. Arrows indicate direction of aerosol flow. Blue dots on PGC indicate aerosol particles.

3. Results and Discussion

3.1. Effect of Low (<2%) RH on NPF

Chamber experiments were undertaken to systematically probe the role of RH on NPF and C_{SOA} generation from the dark ozonolysis of CHA. The numerical results are summarized above in Table 1. Note that the experiment was run in triplicate only for the case of the dry conditions (0.0% RH). Owing to the difficulty in reproducing an exact RH

at such low levels, all experiments with any humidity present were performed only once. Nonetheless, we have demonstrated in a previous report [43] that the typical reproducibility utilizing our optimized setup is better than 10% relative standard deviation.

Table 1. Maximum particle number density (N_{max}), SOA mass ($C_{SOA,max}$), and particle geometric mean diameter (GMD_{max}) measured for each experiment. Each value was normalized (indicated by *) to those measured at 0% RH. ξ_{CHA} and ξ_{O3} are the CHA and O_3 mixing ratios (ppb_v), respectively. n = 3 for the dry experiment at 0.0% RH, and n = 1 for all other runs. Typical relative standard deviation for each metric is less than 10%, as demonstrated in a separate report [43].

RH (%)	ξ_{CHA} (ppb_v)	ξ_{O3} (ppb_v)	N_{max} (10^3 cm^{-3})	N_{max} *	$C_{SOA,max}$ ($\mu g\ m^{-3}$)	$C_{SOA,max}$ *	GMD_{max} (nm)	GMD_{max} *
0.0	99.5	297.7	89.2	1	31.5	1	83.5	1
0.07_0	99.2	302.4	69.8	0.78	35.0	1.11	92.5	1.11
0.09_4	99.9	293.2	57.2	0.64	30.6	0.97	93.6	1.12
0.16_9	98.6	295.6	38.7	0.43	29.8	0.95	104.8	1.26
0.19_9	99.6	284.0	34.6	0.39	31.8	1.01	113.4	1.36
0.39_3	100.3	294.0	20.6	0.23	29.2	0.93	126.9	1.52
0.59_1	100.1	297.1	18.5	0.21	12.2	0.39	181.3	2.17
1.5	99.2	292.3	0.1	0.002	0.78	0.025	199.8	2.39

For the case of CHA, even slight increases in RH (<0.1%) at particle genesis resulted in reductions in NPF (Figure 3). A similar trend was observed for C_{SOA} produced under dry and humid conditions. However, the attenuation of NPF appears to be more sensitive to RH compared to C_{SOA}. This effect may be due, in part, to enhanced partitioning of semi-volatile (SV) and low-volatility (LV) oxidation products to the organic particulate under humid conditions.

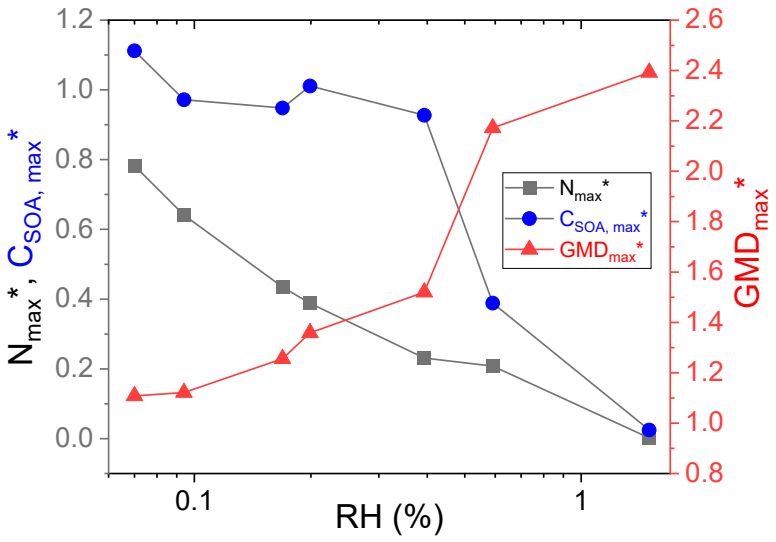

Figure 3. Semi-log plot of relative changes in N_{max}* (black), $C_{SOA,max}$* (blue) and GMD_{max}* (red) measured as a function of relative humidity at particle genesis. All values are normalized to those measured at 0.0% RH. Lines are drawn to aid the eye. n = 1.

Assuming the organic particles remain liquid, the uptake of gas-phase compounds follows an absorptive mechanism (not simple surface condensation). Under these conditions, the partitioning of gas-phase compounds to the particulate can be approximated by

the partition coefficient (K_p), which describes the equilibrium concentration of oxidation products in the gas and particle phases. K_p is given by [46,47]

$$K_p = \frac{760RT\ f_{om}}{10^6\ MW_{om}\zeta\ \rho_L^0}$$

where R (m^3 atm mol^{-1} K^{-1}) is the ideal gas constant; T (K) is the temperature; f_{om} is the weight fraction of the particulate that comprises the absorbing organic material (om) phase; MW_{om} (g mol^{-1}) is the average molecular weight of the absorbing om phase; ζ is the activity coefficient; and ρ_L^0 (Torr) is the saturation vapor pressure of the compound as a liquid. Each ζ is a function of the composition of the aerosol mixture and the temperature, and each ρ_L^0 is a strong function of the temperature. Increased liquid water content within the organic particulate will decrease the average molecular weight of the organic matter, thereby favoring SOA partitioning (K_p) [46,47] as RH increases. This hypothesis is supported by the increased GMD_{max} with increasing RH (Table 1). Similar enhancements in organic aerosol mass were reported for SOA generated from the dark ozonolysis of α-pinene at atmospherically relevant mass loadings [48]. This same conclusion is suggested by the apparent leveling off of the SOA mass loss (C_{SOA}*) at the highest RHs (lowest mass loadings).

In addition, Figure 4a,b shows the ELPI+ time evolution of CHA-derived SOA number and size distributions for 12 and 2 h of flushing, respectively, after having humidified the chamber to 60% RH. With less flushing, the magnitude of N decreased by more than an order of magnitude, while the GMD distribution shifted to greater sizes (fewer, larger particles; in support of experiments from Table 1). This demonstrated that CHA, as a chemical precursor to aerosol formation, is so sensitive to water that even miniscule amounts of water (where the RH sensor read 0.0%) left in the chamber from a previous experiment was sufficient to impact the chemical formation of CHA-derived SOA in a subsequent experiment.

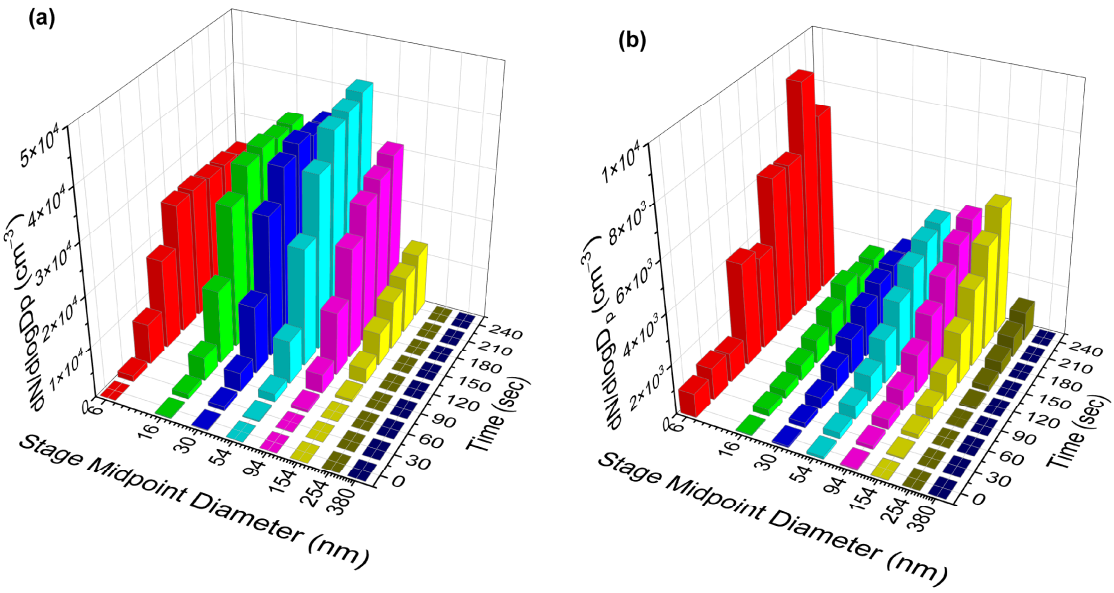

Figure 4. Time evolution of CHA-derived SOA particle number distributions following chamber humidification and subsequent dry flushing. (**a**) 12 h of dry flushing; (**b**) 2 h of dry flushing. For both, SOA was generated at RH = 0% (as measured by the RH sensor), ξ_{VOC} = 150 ppb_v, ξ_{O3} = 500 ppb_v. n = 1.

3.2. Effect of Solubility on Decreased NPF

Decreased NPF as a function of increasing RH may be due to enhanced losses of CHA, a water-soluble GLV, and/or its oxidation products onto the chamber walls. Under conditions

of high humidity, water vapor will adsorb/absorb onto/into the walls of the chamber, forming a thin aqueous layer into which CHA could dissolve. For example, Teflon® can adsorb/absorb 1–10 mg of water per dm^2 of surface area at >90% RH [49–52], which for the UVMEC used in this study (24 m^2 internal surface area) suggests a total water content on/in the walls of 2.4–24 g. Considering the aqueous solubility of CHA (0.9 g/L [53]), this is sufficient water to solubilize up to 2.2–22 mg of CHA, which is significant compared to the total amount of CHA injected for a typical experiment (e.g., 270 ppb_v = 11.8 mg).

To test this hypothesis, experiments were conducted whereby the amount of chamber wall water was varied by the control of chamber flushing with dry, particle-free air. For these experiments, the UVMEC was humidified to 60% RH and allowed to equilibrate for 60 min. With an estimated water adsorption time constant of 3.8 min [52], this was sufficient to saturate the chamber walls with water. The desorption time constant (τ_d) has been estimated to be 90 min [52]. Different levels of residual water loadings remaining on the chamber walls were then achieved by flushing for 1.5, 12 and 60 h. It is interesting to note that after flushing for 1.5 h (τ_d = 1) after humidification/equilibration, the measured RH in the *sealed* chamber (static conditions, no flushing) slowly increased from 0% to 2% over the course of an additional hour. Therefore, any experiment that was run after only a short period of flushing (less than 2–3 τ_d), could be considered the same as running it at an RH of a few %. No increase in RH was measured over time after flushing the chamber for more than 48 h (i.e., there was no measurable residual water remaining on the chamber walls after the extended flushing period). With this, a final experiment was conducted, wherein after flushing the chamber for 60 h and re-humidification to 2% RH (which should result in negligible wall water), the experiment was run again. The results (Figure 5) indicate the recovery of SOA formation (both NPF and SOA mass) as a function of chamber flushing.

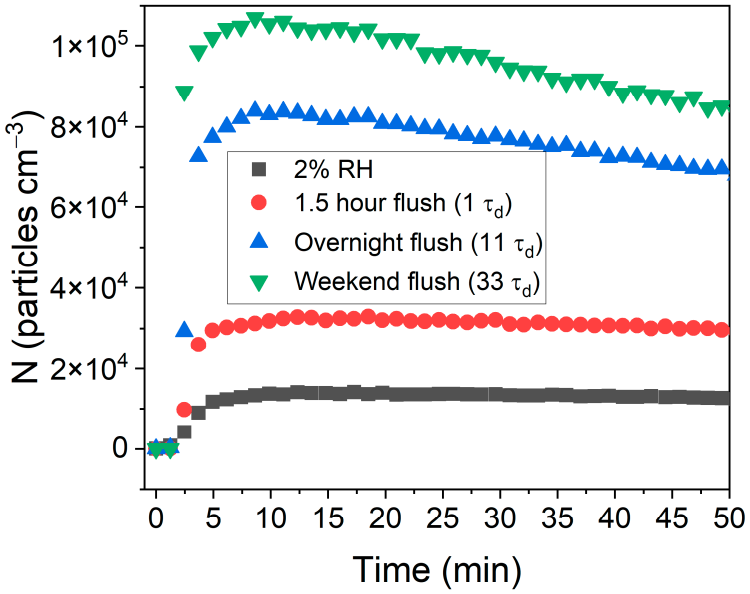

Figure 5. SOA evolution as a function of variable wall water. ξ_{CHA} = 150 ppb_v and ξ_{VOC} = 500 ppb_v. n = 1.

Furthermore, when the RH was brought up to 2% RH (from a completely dry chamber, following a 60 h flushing period), SOA formation closely approximated that after flushing for only 1.5 h. Note that for the 1.5 h flush experiment, CHA was injected while the RH sensor indicated a nominal RH of 0.0%. Unfortunately, instrumental enhancements that permit the measurement of RH with a resolution of 0.01% (as shown in Table 1) had not yet been implemented. We now know that due to the poorer resolution used for the ELPI+ measurements, the RH in the UVMEC could have been as high as 0.5% before the RH sensor would indicate 1.0%. It follows, therefore, that we would expect N_{max} obtained at

2% RH (which in reality could have been anywhere between 1.5% and 2.5%) to be lower than after the 1.5 h flush. This suggests that, for CHA, the reduction in NPF and C_{SOA} is not due to solubility, but rather primarily due to gas-phase chemistry in the presence of water vapor.

3.3. Water-Facilitated Chemistry

Using NIR-LDI-AMS chemical analysis of the CHA-derived SOA, we observe differences in product profiles between aerosol formed under dry and humid conditions. A brief description of the ozonolysis reaction pathway (Scheme 1) is helpful to better understand potential pathways leading to these RH-induced oxidation products and the ensuing discussion.

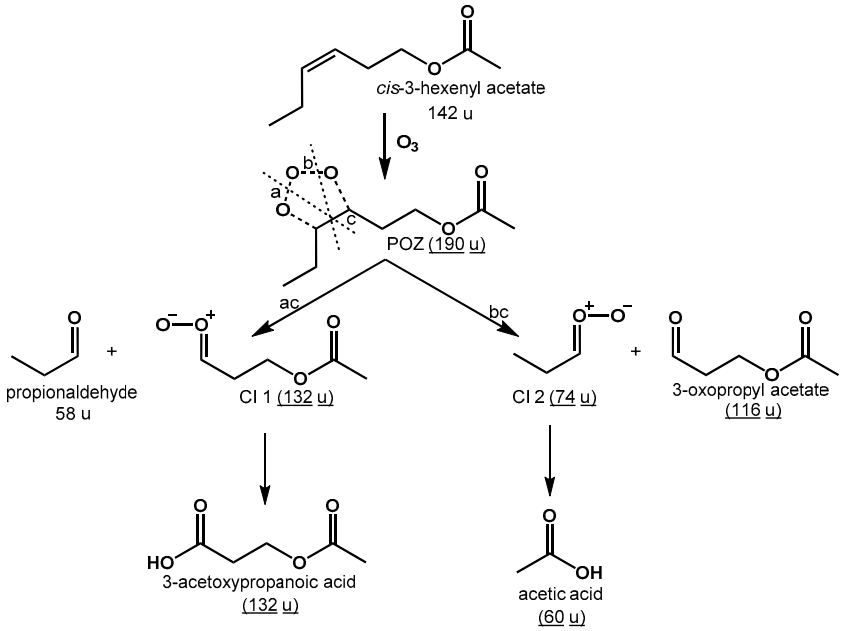

Scheme 1. Mechanism for the electrophilic addition of ozone to *cis*-3-hexenyl acetate (CHA) and subsequent cleavage of the primary ozonide (POZ) [14].

Upon the cycloaddition of ozone to CHA, the primary ozonide will decompose to yield a stable aldehyde and an excited Criegee intermediate (CI). The CIs can be energetically stabilized, which allows for further reactions, leading to the formation of low-volatility highly oxygenated molecules (HOMs), which contribute to NPF [28,32,54–61]. SOA formation is often discussed in terms of a competition between nucleation (NPF) and condensation (growth, in terms of mass). In other words, oxidative products of higher volatility may be less likely to nucleate to form new particles but will still contribute to overall C_{SOA} through condensational growth. On the other hand, products of sufficiently low volatility, such as dimers of CIs of at least 10 carbons each (as in the case of cyclic monoterpenes (C10-CI dimers) [28,32,54–60,62,63] and highly oxidized products generated via autoxidation [54,55,58,64–71], would favor NPF. In the case of CHA, our results suggest that water negatively affects both SOA processes (nucleation and condensation). As the gas-phase water concentration increases, more of the CHA-derived CIs (henceforth referred to as C5-CIs) are quenched and diverted away from subsequent reactions that could lead to low volatility products, which act as nucleating agents to enhance NPF; therefore, the quenching reaction with water for C5-CIs would decrease NPF events. Additionally, because the SOA mass continues to decrease at higher RH, it appears that the products from the quenched C5-CIs are of relatively high volatility and participate less effectively in condensational growth as well.

Computational and experimental studies have predicted that smaller CIs are more reactive toward water [63,72–81]; therefore, it is possible that the C5-CIs are depleted before multigenerational chemical pathways are activated and a significant supersaturation of extremely low-volatility gas-phase products (ELVOCs) formed is large enough to result in NPF. Reducing ELVOCs would likely shift the balance between NPF and C_{SOA} toward the latter, resulting in fewer, larger particles (increased GMD, Table 1). To better understand the chemical processes leading to this observation, NIR-LDI-AMS was deployed to provide insight into composition changes of the SOA affected by the presence of water vapor at particle genesis.

3.4. Proposed Chemical Mechanisms

A mechanistic description for the formation of products from the ozonolysis of CHA has been presented elsewhere [14]. As seen in Scheme 1, the electrophilic addition of ozone across the double bond produces a primary ozonide (POZ), which decomposes to yield four fragments. Two of the products are closed shell aldehydes, while the other two are energetic alkylperoxide CIs that can unimolecularly rearrange to the carboxylic acids or be stabilized and participate in subsequent, multigenerational products.

Observationally, we see that the mass spectrum derived under humid conditions differs from that under dry conditions (Figure 6). Specifically, under humid conditions, newly dominant products are recorded at 147, 203, 261, 317, 319, and 347 m/z. Scheme 2a,b proposes rational mechanisms leading to some of these products.

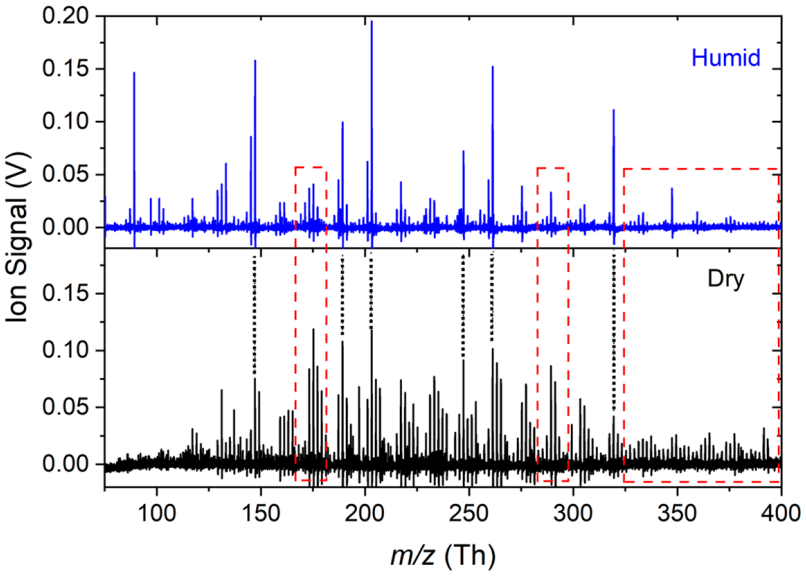

Figure 6. Soft ionization mass spectra of CHA-derived SOA generated under dry and humid conditions. Dashed boxes (red) indicate mass spectral features attenuated in presence of RH. Dotted lines (black) highlight specific molecular products enhanced through by RH.

Based upon the current literature reports and estimated VPs for these pure compounds (Table 2), one would expect that these heavier MW products would be of sufficiently low VP to contribute to NPF [56,82], contrary to our observation. This suggests that either the vapor-phase concentration of these products does not reach supersaturation, and hence does not form new particles, or that there exists another mechanism(s), physical or chemical, that results in decreased NPF rates and overshadows any enhanced NPF due to these products. As such, while interesting, it is not likely that the deviations in chemical pathways described here (that are induced by water vapor) can explain the observed behavior.

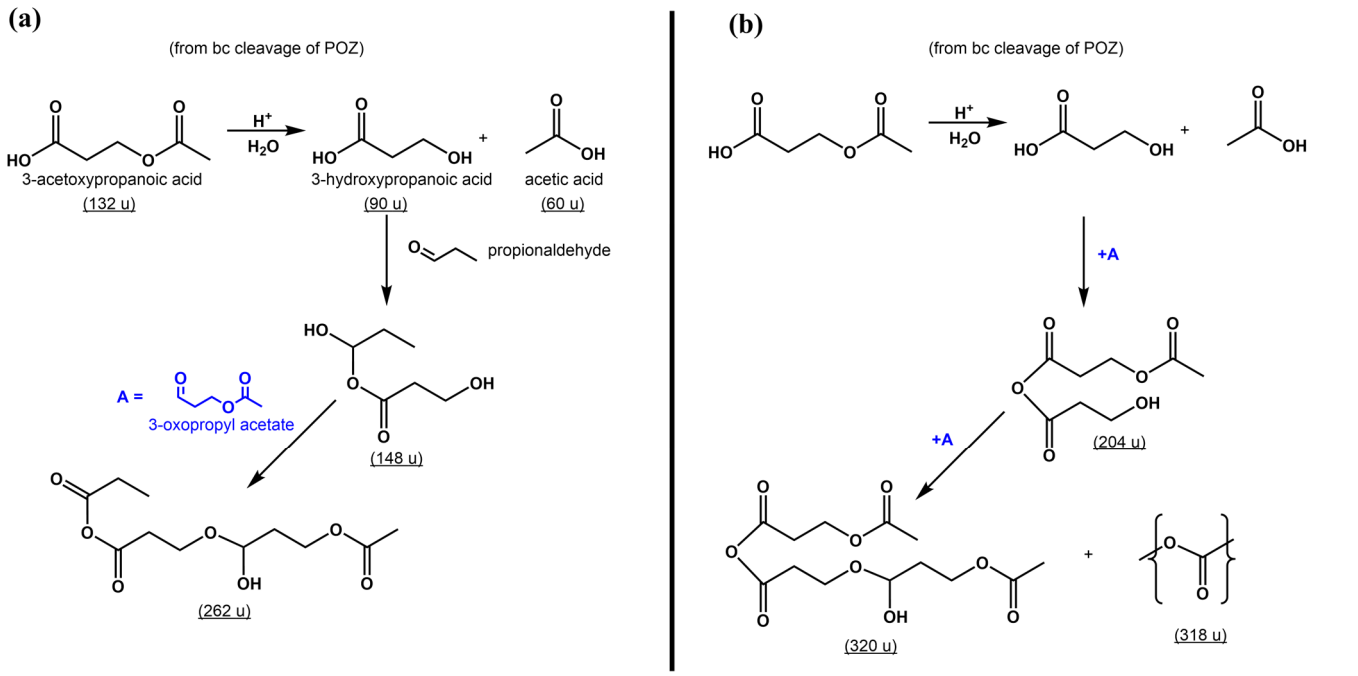

Scheme 2. Proposed mechanisms for the formation of water-derived SOA products in the ozonolysis of CHA under humid conditions: (**a**) 262 u and (**b**) 204, 318 and 320 u.

Table 2. Estimated vapor pressures for products of CHA ozonolysis dominant under humid conditions.

Product MW ($g\ mol^{-1}$)	Estimated VP (Pa)	Volatility Class
148	10^{-2}	IVOC
184 (pinonic acid)	10^{-3}	SVOC
204	10^{-4}	SVOC
262	10^{-8}	LVOC
318	10^{-10}	ELVOC
320	10^{-13}	ULVOC
348 *	10^{-15}	ULVOC

Vapor pressures were estimated using UManSysPro (http://umansysprop.seaes.manchester.ac.uk/tool/vapour_pressure, accessed on 7 March 2023). ULVOCs (shaded cells) are considered necessary for homogeneous NPF. * VP estimated based on adding 2 -CH_2- units or one -C=O unit to 320 product.

3.5. Quaternary System Experiments

In contrast to CHA, α-pinene shows only a slight decrease in NPF, while SOA mass remains constant [26–31]. Due to the cyclic alkene in α-pinene, the ozonolysis of the endocyclic double bond results in a single C10-CI that is much larger and heavier and with a lower VP than the CHA-derived CIs. Therefore, unlike CHA-derived SOA, the stabilized CI products are of sufficient VP to partition to existing SOA and will also favor secondary reactions, such as dimerization and autoxidation, which contribute to NPF and C_{SOA}. The question remains however, whether the quenching of the C5-CIs in the CHA system with water outcompetes oligomerization and autoxidation reactions, leading to a decrease in NPF. To answer this question, experiments were conducted using a quaternary system of α-pinene, CHA, water vapor, and ozone.

In a manner analogous to Heinritzi et al. [83], we conducted mixed system experiments using CHA and α-pinene, anticipating that the presence of the small C5-CIs from the ozonolysis of CHA would sequester C10-CIs from α-pinene, preventing the formation of C20-dimers necessary for NPF. We have shown previously that gas-phase water does not suppress NPF from α-pinene ozonolysis at low ξ_{VOC} [26]. Therefore, if CHA reduces

α-pinene-derived SOA formation, and CHA CIs are efficiently sequestered by water, then the addition of water vapor to this quaternary system should aid in recovering SOA formation from α-pinene ozonolysis (Table 3). In other words, CIs are competing between a reaction with water or a reaction with another CI. If the C5-CI reaction with water is faster, then an increase in NPF will result. If, on the other hand, intermolecular reactions involving the C5-CIs are faster, then the resulting dimers/oligomers are less likely to contribute to NPF and C_{SOA}.

Table 3. Results of NPF and SOA formation from quaternary system of α-pinene, CHA and O_3 with and without added humidity. n = 1.

$\xi_{\alpha\text{-Pinene:CHA:RH}}$	α-Pinene (ppb_v)	CHA (ppb_v)	%RH	Ozone (ppb_v)	N_{max} ($\times 10^3$) (#/cm^3)	ΔN_{max} *	C_{SOA} (μg/m^3)	GMD (nm)
$\xi_{6:0:0}$	6	0	0	500	32.7	−82%	4.32	49.9
$\xi_{6:12:0}$	6	12	0	500	5.8		2.33	64.5
$\xi_{6:0:60}$	6	0	60	500	144	−20%	11.5	49.1
$\xi_{6:12:60}$	6	12	60	500	115		6.89	43.9

* ΔN_{max} describes the relative decrease in N_{max} in the presence of CHA under dry and humid conditions.

Comparing $\xi_{6:0:0}$ and $\xi_{6:12:0}$ ($\xi_{\alpha\text{-pinene:CHA:RH}}$) supports the observation of Heinritzi et al. [83] in that the addition of a source of small CIs reduces NPF from the monoterpene by 82%. It should be noted that in a binary system of CHA and O_3, no particles are formed at the ξ_{CHA} used here. We also observed that the GMD increases significantly when CHA is present, likely due to the partitioning of CHA ozonolysis products, as well as C15 products from the cross coupling of the C5 and C10-CIs to α-pinene SOA. While the addition of water does not result in the full recovery of α-pinene SOA (compare $\xi_{6:0:60}$ and $\xi_{6:12:60}$), with a remaining net reduction in NPF of 20%, the reduced GMD under humid conditions suggests that SOA mass for the quaternary system under humid conditions arises primarily from NPF and not simply from particle growth (through the partitioning of S- and LVOCs).

4. Conclusions

Herein we report on experiments to elucidate the impact and role of gaseous water at particle genesis on NPF and C_{SOA} from the ozonolysis of the green-leaf volatile CHA. We demonstrate that at ξ_{CHA} = 100 ppb_v and at RHs as low as 1.5%, NPF is effectively shut down for this SOA precursor. At lower RHs, NPF appears to be more sensitive to RH than does C_{SOA}. NPF from α-pinene ozonolysis at similar ξ_{VOCs}, on the other hand, remained insensitive to the presence of RH, in accord with previous reports [26,27,84–86]. We also present evidence to demonstrate that the effective shutdown of particle formation for CHA-derived SOA in the presence of water is not a physical process but rather is due to gaseous water playing an important role in the chemical mechanism and leading to the shutdown of NPF.

Even at low RHs (<2%), there were marked decreases in SOA production (NPF and C_{SOA}) with fewer, larger particles being formed. Although the estimated vapor pressures of the formed gas-phase products should be sufficiently low to nucleate and contribute to NPF, we observed a dramatic decrease in SOA production even when little water was present (0.07% RH led to a 21.7% decrease in particle formation). Therefore, we suggest that the Criegee intermediates formed upon the ozonolysis of CHA are quenched by the gaseous water, which subsequently do not nucleate and contribute to NPF. Our findings, in tandem with our recent observations with α- and β-pinene [26], suggest that gaseous water, the third most abundant atmospheric gas, plays a vital role in the mechanistic formation of atmospheric aerosols.

Author Contributions: A.C.F. carried out all humidity vs. particle formation experiments, ELPI+ experiments, and solubility experiments. C.N.S. carried out quaternary system experiments and mass spectral analysis. G.A.P. conceptualized this work and supervised all laboratory activities. G.A.P. prepared the original manuscript draft, and all authors contributed to the writing and editing of the final manuscript. All authors have read and agreed to the published version of the manuscript.

Funding: This material is based upon work supported by the National Science Foundation under Grant No. CHE-1709751.

Institutional Review Board Statement: Not applicable.

Informed Consent Statement: Not applicable.

Data Availability Statement: The data presented in this study are available on request from the corresponding author.

Conflicts of Interest: The authors declare no conflict of interest.

References

1. Kanakidou, M.; Seinfeld, J.H.; Pandis, S.N.; Barnes, I.; Dentener, F.J.; Facchini, M.C.; Van Dingenen, R.; Ervens, B.; Nenes, A.; Nielsen, C.J.; et al. Organic aerosol and global climate modelling: A review. *Atmos. Chem. Phys.* **2005**, *5*, 1053–1123. [CrossRef]
2. Hallquist, M.; Wenger, J.C.; Baltensperger, U.; Rudich, Y.; Simpson, D.; Claeys, M.; Dommen, J.; Donahue, N.M.; George, C.; Goldstein, A.H.; et al. The formation, properties and impact of secondary organic aerosol: Current and emerging issues. *Atmos. Chem. Phys.* **2009**, *9*, 5155–5236. [CrossRef]
3. Guenther, A.B.; Jiang, X.; Heald, C.L.; Sakulyanontvittaya, T.; Duhl, T.; Emmons, L.K.; Wang, X. The Model of Emissions of Gases and Aerosols from Nature version 2.1 (MEGAN2.1): An extended and updated framework for modeling biogenic emissions. *Geosci. Model. Dev.* **2012**, *5*, 1471–1492. [CrossRef]
4. Wiedinmyer, C.; Guenther, A.; Harley, P.; Hewitt, N.; Geron, C.; Artaxo, P.; Steinbrecher, R.; Rasmussen, R. *Global Organic Emissions from Vegetation*; Springer: Dordrecht, The Netherlands, 2004; pp. 115–170.
5. Mahilang, M.; Deb, M.K.; Pervez, S. Biogenic secondary organic aerosols: A review on formation mechanism, analytical challenges and environmental impacts. *Chemosphere* **2021**, *262*, 127771. [CrossRef] [PubMed]
6. Cao, J.; Situ, S.; Hao, Y.F.; Xie, S.D.; Li, L.Y. Enhanced summertime ozone and SOA from biogenic volatile organic compound (BVOC) emissions due to vegetation biomass variability during 1981–2018 in China. *Atmos. Chem. Phys.* **2022**, *22*, 2351–2364. [CrossRef]
7. Sarang, K.; Rudzinski, K.J.; Szmigielski, R. Green Leaf Volatiles in the Atmosphere-Properties, Transformation, and Significance. *Atmosphere* **2021**, *12*, 1655. [CrossRef]
8. Barreira, L.M.F.; Ylisirnio, A.; Pullinen, I.; Buchholz, A.; Li, Z.J.; Lipp, H.; Junninen, H.; Horrak, U.; Noe, S.M.; Krasnova, A.; et al. The importance of sesquiterpene oxidation products for secondary organic aerosol formation in a springtime hemiboreal forest. *Atmos. Chem. Phys.* **2021**, *21*, 11781–11800. [CrossRef]
9. Bianchi, F.; Junninen, H.; Bigi, A.; Sinclair, V.A.; Dada, L.; Hoyle, C.R.; Zha, Q.; Yao, L.; Ahonen, L.R.; Bonasoni, P.; et al. Biogenic particles formed in the Himalaya as an important source of free tropospheric aerosols. *Nat. Geosci.* **2021**, *14*, 4–9. [CrossRef]
10. Donahue, N.M.; Ortega, I.K.; Chuang, W.; Riipinen, I.; Riccobono, F.; Schobesberger, S.; Dommen, J.; Baltensperger, U.; Kulmala, M.; Worsnop, D.R.; et al. How do organic vapors contribute to new-particle formation? *Faraday Discuss.* **2013**, *165*, 91–104. [CrossRef]
11. Kammer, J.; Flaud, P.M.; Chazeaubeny, A.; Ciuraru, R.; Le Menach, K.; Geneste, E.; Budzinski, H.; Bonnefond, J.M.; Lamaud, E.; Perraudin, E.; et al. Biogenic volatile organic compounds (BVOCs) reactivity related to new particle formation (NPF) over the Landes forest. *Atmos. Res.* **2020**, *237*, 104869. [CrossRef]
12. Wiedensohler, A.; Ma, N.; Birmili, W.; Heintzenberg, J.; Ditas, F.; Andreae, M.O.; Panov, A. Infrequent new particle formation over the remote boreal forest of Siberia. *Atmos. Environ.* **2019**, *200*, 167–169. [CrossRef]
13. Zhao, B.; Shrivastava, M.; Donahue, N.M.; Gordon, H.; Schervish, M.; Shilling, J.E.; Zaveri, R.A.; Wang, J.; Andreae, M.O.; Zhao, C.; et al. High concentration of ultrafine particles in the Amazon free troposphere produced by organic new particle formation. *Proc. Natl. Acad. Sci. USA* **2020**, *117*, 25344–25351. [CrossRef] [PubMed]
14. Jain, S.; Zahardis, J.; Petrucci, G.A. Soft Ionization Chemical Analysis of Secondary Organic Aerosol from Green Leaf Volatiles Emitted by Turf Grass. *Environ. Sci. Technol.* **2014**, *48*, 4835–4843. [CrossRef] [PubMed]
15. Harvey, R.M.; Bateman, A.P.; Jain, S.; Li, Y.J.; Martin, S.; Petrucci, G.A. Optical Properties of Secondary Organic Aerosol from cis-3-Hexenol and cis-3-Hexenyl Acetate: Effect of Chemical Composition, Humidity, and Phase. *Environ. Sci. Technol.* **2016**, *50*, 4997–5006. [CrossRef] [PubMed]
16. Artaxo, P.; Hansson, H.C.; Andreae, M.O.; Back, J.; Alves, E.G.; Barbosa, H.M.J.; Bender, F.; Bourtsoukidis, E.; Carbone, S.; Chi, J.S.; et al. Tropical and Boreal Forest Atmosphere Interactions: A Review. *Tellus B* **2022**, *74*, 24–163. [CrossRef]
17. Donahue, N.M.; Robinson, A.L.; Pandis, S.N. Atmospheric organic particulate matter: From smoke to secondary organic aerosol. *Atmos. Environ.* **2009**, *43*, 94–106. [CrossRef]

18. Harvey, R.M.; Zahardis, J.; Petrucci, G.A. Establishing the contribution of lawn mowing to atmospheric aerosol levels in American suburbs. *Atmos. Chem. Phys.* **2014**, *14*, 797–812. [CrossRef]
19. Porter, W.C.; Jimenez, J.L.; Barsanti, K.C. Quantifying Atmospheric Parameter Ranges for Ambient Secondary Organic Aerosol Formation. *ACS Earth Space Chem.* **2021**, *5*, 2380–2397. [CrossRef]
20. Lampilahti, J.; Manninen, H.E.; Nieminen, T.; Mirme, S.; Ehn, M.; Pullinen, I.; Leino, K.; Schobesberger, S.; Kangasluoma, J.; Kontkanen, J.; et al. Zeppelin-led study on the onset of new particle formation in the planetary boundary layer. *Atmos. Chem. Phys.* **2021**, *21*, 12649–12663. [CrossRef]
21. Franco, M.A.; Ditas, F.; Kremper, L.A.; Machado, L.A.T.; Andreae, M.O.; Araújo, A.; Barbosa, H.M.J.; de Brito, J.F.; Carbone, S.; Holanda, B.A.; et al. Occurrence and growth of sub-50 nm aerosol particles in the Amazonian boundary layer. *Atmos. Chem. Phys.* **2022**, *22*, 3469–3492. [CrossRef]
22. Lee, S.H.; Gordon, H.; Yu, H.; Lehtipalo, K.; Haley, R.; Li, Y.X.; Zhang, R.Y. New Particle Formation in the Atmosphere: From Molecular Clusters to Global Climate. *J. Geophys. Res.-Atmos.* **2019**, *124*, 7098–7146. [CrossRef]
23. Baalbaki, R.; Pikridas, M.; Jokinen, T.; Laurila, T.; Dada, L.; Bezantakos, S.; Ahonen, L.; Neitola, K.; Maisser, A.; Bimenyimana, E.; et al. Towards understanding the characteristics of new particle formation in the Eastern Mediterranean. *Atmos. Chem. Phys.* **2021**, *21*, 9223–9251. [CrossRef]
24. Zimmerman, A.; Petters, M.D.; Meskhidze, N. Observations of new particle formation, modal growth rates, and direct emissions of sub-10 nm particles in an urban environment. *Atmos. Environ.* **2020**, *242*, 117835. [CrossRef] [PubMed]
25. Sulo, J.; Sarnela, N.; Kontkanen, J.; Ahonen, L.; Paasonen, P.; Laurila, T.; Jokinen, T.; Kangasluoma, J.; Junninen, H.; Sipila, M.; et al. Long-term measurement of sub-3 nm particles and their precursor gases in the boreal forest. *Atmos. Chem. Phys.* **2021**, *21*, 695–715. [CrossRef]
26. Snyder, C.N.; Flueckiger, A.C.; Petrucci, G.A. Relative Humidity Impact on Organic New Particle Formation from Ozonolysis of α- and β-Pinene at Atmospherically Relevant Mixing Ratios. *Atmosphere* **2023**, *14*, 173. [CrossRef]
27. Jonsson, A.M.; Hallquist, M.; Ljungstrom, E. Impact of humidity on the ozone initiated oxidation of limonene, Delta(3)-carene, and alpha-pinene. *Environ. Sci. Technol.* **2006**, *40*, 188–194. [CrossRef] [PubMed]
28. Li, X.X.; Chee, S.; Hao, J.M.; Abbatt, J.P.D.; Jiang, J.K.; Smith, J.N. Relative humidity effect on the formation of highly oxidized molecules and new particles during monoterpene oxidation. *Atmos. Chem. Phys.* **2019**, *19*, 1555–1570. [CrossRef]
29. Pommer, L.; Fick, J.; Andersson, B.; Nilsson, C. The influence of O-3, relative humidity, NO and NO_2 on the oxidation of alpha-pinene and Delta(3)-carene. *J. Atmos. Chem.* **2004**, *48*, 173–189. [CrossRef]
30. Ma, Y.; Russell, A.T.; Marston, G. Mechanisms for the formation of secondary organic aerosol components from the gas-phase ozonolysis of alpha-pinene. *Phys. Chem. Chem. Phys.* **2008**, *10*, 4294–4312. [CrossRef]
31. Emanuelsson, E.U.; Watne, A.K.; Lutz, A.; Ljungstrom, E.; Hallquist, M. Influence of Humidity, Temperature, and Radicals on the Formation and Thermal Properties of Secondary Organic Aerosol (SOA) from Ozonolysis of beta-Pinene. *J. Phys. Chem. A* **2013**, *117*, 10346–10358. [CrossRef]
32. Caudillo, L.; Rorup, B.; Heinritzi, M.; Marie, G.; Simon, M.; Wagner, A.C.; Muller, T.; Granzin, M.; Amorim, A.; Ataei, F.; et al. Chemical composition of nanoparticles from alpha-pinene nucleation and the influence of isoprene and relative humidity at low temperature. *Atmos. Chem. Phys.* **2021**, *21*, 17099–17114. [CrossRef]
33. Yu, K.P.; Lin, C.C.; Yang, S.C.; Zhao, P. Enhancement effect of relative humidity on the formation and regional respiratory deposition of secondary organic aerosol. *J. Hazard. Mater.* **2011**, *191*, 94–102. [CrossRef] [PubMed]
34. Hamed, A.; Korhonen, H.; Sihto, S.L.; Joutsensaari, J.; Jarvinen, H.; Petaja, T.; Arnold, F.; Nieminen, T.; Kulmala, M.; Smith, J.N.; et al. The role of relative humidity in continental new particle formation. *J. Geophys. Res.-Atmos.* **2011**, *116*, D03202. [CrossRef]
35. Li, J.J.; Wang, G.H.; Cao, J.J.; Wang, X.M.; Zhang, R.J. Observation of biogenic secondary organic aerosols in the atmosphere of a mountain site in central China: Temperature and relative humidity effects. *Atmos. Chem. Phys.* **2013**, *13*, 11535–11549. [CrossRef]
36. Liang, L.L.; Engling, G.; Cheng, Y.; Zhang, X.Y.; Sun, J.Y.; Xu, W.Y.; Liu, C.; Zhang, G.; Xu, H.; Liu, X.Y.; et al. Influence of High Relative Humidity on Secondary Organic Carbon: Observations at a Background Site in East China. *J. Meteorol. Res.* **2019**, *33*, 905–913. [CrossRef]
37. von Hessberg, C.; von Hessberg, P.; Poschl, U.; Bilde, M.; Nielsen, O.J.; Moortgat, G.K. Temperature and humidity dependence of secondary organic aerosol yield from the ozonolysis of beta-pinene. *Atmos. Chem. Phys.* **2009**, *9*, 3583–3599. [CrossRef]
38. Zhao, Z.X.; Le, C.; Xu, Q.; Peng, W.H.; Jiang, H.H.; Lin, Y.H.; Cocker, D.R.; Zhang, H.F. Compositional Evolution of Secondary Organic Aerosol as Temperature and Relative Humidity Cycle in Atmospherically Relevant Ranges. *ACS Earth Space Chem.* **2019**, *3*, 2549–2558. [CrossRef]
39. Geddes, S.; Nichols, B.; Todd, K.; Zahardis, J.; Petrucci, G.A. Near-infrared laser desorption/ionization aerosol mass spectrometry for measuring organic aerosol at atmospherically relevant aerosol mass loadings. *Atmos. Meas. Tech.* **2010**, *3*, 1175–1183. [CrossRef]
40. Nakao, S.; Tang, P.; Tang, X.C.; Clark, C.H.; Qi, L.; Seo, E.; Asa-Awuku, A.; Cocker, D. Density and elemental ratios of secondary organic aerosol: Application of a density prediction method. *Atmos. Environ.* **2013**, *68*, 273–277. [CrossRef]
41. Geddes, S.; Nichols, B.; Flemer, S.; Eisenhauer, J.; Zahardis, J.; Petrucci, G.A. Near-Infrared Laser Desorption/Ionization Aerosol Mass Spectrometry for Investigating Primary and Secondary Organic Aerosols under Low Loading Conditions. *Anal. Chem.* **2010**, *82*, 7915–7923. [CrossRef]
42. Presto, A.A.; Huff Hartz, K.E.; Donahue, N.M. Secondary Organic Aerosol Production from Terpene Ozonolysis. 1. Effect of UV Radiation. *Environ. Sci. Technol.* **2005**, *39*, 7036–7045. [CrossRef]

43. Flueckiger, A.; Petrucci, G.A. Methodological advances to improve repeatability of SOA generation in enivronmental chambers. *Aerosol. Sci. Technol.* **2023**, *57*, 925–933. [CrossRef]
44. Masi, J.M. Artificial Growth of Aerosol Particles for Mass Spectrometry Measurement. Bachelor's Thesis, University of Vermont, Burlington, VT, USA, 2020.
45. Kerecman, D.E.; Apsokardu, M.J.; Talledo, S.L.; Taylor, M.S.; Haugh, D.N.; Zhang, Y.; Johnston, M.V. Online Characterization of Organic Aerosol by Condensational Growth into Aqueous Droplets Coupled with Droplet-Assisted Ionization. *Anal. Chem.* **2021**, *93*, 2793–2801. [CrossRef] [PubMed]
46. Pankow, J.F.; Marks, M.C.; Barsanti, K.C.; Mahmud, A.; Asher, W.E.; Li, J.Y.; Ying, Q.; Jathar, S.H.; Kleeman, M.J. Molecular view modeling of atmospheric organic particulate matter: Incorporating molecular structure and co-condensation of water. *Atmos. Environ.* **2015**, *122*, 400–408. [CrossRef]
47. Seinfeld, J.H.; Erdakos, G.B.; Asher, W.E.; Pankow, J.F. Modeling the formation of secondary organic aerosol (SOA). 2. The predicted effects of relative humidity on aerosol formation in the alpha-pinene-, beta-pinene-, sabinene-, Delta(3)-Carene-, and cyclohexene-ozone systems. *Environ. Sci. Technol.* **2001**, *35*, 1806–1817. [CrossRef]
48. Surdu, M.; Lamkaddam, H.; Wang, D.S.; Bell, D.M.; Xiao, M.; Lee, C.P.; Li, D.; Caudillo, L.; Marie, G.; Scholz, W.; et al. Molecular Understanding of the Enhancement in Organic Aerosol Mass at High Relative Humidity. *Environ. Sci. Technol.* **2023**, *57*, 2297–2309. [CrossRef]
49. Dixon, M.; Grace, J. Water-Uptake by Some Chamber Materials. *Plant Cell Environ.* **1982**, *5*, 323–327. [CrossRef]
50. Sacher, E.; Susko, J.R. Water Permeation of Polymer Films. IV. Teflon FEP. *J. Appl. Polym. Sci.* **1982**, *27*, 3893–3902. [CrossRef]
51. Shepherd, W. Moisture Absorption by Some Instrumental Materials. *Rev. Sci. Instrum.* **1973**, *44*, 234. [CrossRef]
52. Liebe, H.J.; Wolfe, V.L.; Howe, D.A. Test of wall coatings for controlled moist air experiments. *Rev. Sci. Instrum.* **1984**, *55*, 1702–1705. [CrossRef]
53. Showing Metabocard for cis-3-Hexenyl Acetate. Human Metabolome Database. Available online: https://hmdb.ca/metabolites/HMDB0040215 (accessed on 24 January 2023).
54. Shi, X.L.; Huang, G.X.Z.; Yang, D.H.; Zhang, Q.Z.; Zong, W.S.; Cheng, J.M.; Sui, X.; Yuan, F.H.; Wang, W.X. Theoretical study of the formation and nucleation mechanism of highly oxygenated multi-functional organic compounds produced by alpha-pinene. *Sci. Total Environ.* **2021**, *780*, 146422. [CrossRef]
55. Simon, M.; Dada, L.; Heinritzi, M.; Scholz, W.; Stolzenburg, D.; Fischer, L.; Wagner, A.C.; Kurten, A.; Rorup, B.; He, X.C.; et al. Molecular understanding of new-particle formation from alpha-pinene between-50 and+25 degrees C. *Atmos. Chem. Phys.* **2020**, *20*, 9183–9207. [CrossRef]
56. Schervish, M.; Donahue, N.M. Peroxy radical chemistry and the volatility basis set. *Atmos. Chem. Phys.* **2020**, *20*, 1183–1199. [CrossRef]
57. Perakyla, O.; Riva, M.; Heikkinen, L.; Quelever, L.; Roldin, P.; Ehn, M. Experimental investigation into the volatilities of highly oxygenated organic molecules (HOMs). *Atmos. Chem. Phys.* **2020**, *20*, 649–669. [CrossRef]
58. Quelever, L.L.J.; Kristensen, K.; Jensen, L.N.; Rosati, B.; Teiwes, R.; Daellenbach, K.R.; Perakyla, O.; Roldin, P.; Bossi, R.; Pedersen, H.B.; et al. Effect of temperature on the formation of highly oxygenated organic molecules (HOMs) from alpha-pinene ozonolysis. *Atmos. Chem. Phys.* **2019**, *19*, 7609–7625. [CrossRef]
59. Qi, X.M.; Ding, A.J.; Roldin, P.; Xu, Z.N.; Zhou, P.T.; Sarnela, N.; Nie, W.; Huang, X.; Rusanen, A.; Ehn, M.; et al. Modelling studies of HOMs and their contributions to new particle formation and growth: Comparison of boreal forest in Finland and a polluted environment in China. *Atmos. Chem. Phys.* **2018**, *18*, 11779–11791. [CrossRef]
60. Bianchi, F.; Trostl, J.; Junninen, H.; Frege, C.; Henne, S.; Hoyle, C.R.; Molteni, U.; Herrmann, E.; Adamov, A.; Bukowiecki, N.; et al. New particle formation in the free troposphere: A question of chemistry and timing. *Science* **2016**, *352*, 1109–1112. [CrossRef] [PubMed]
61. Zhao, Q.L.; Wang, W.N.; Liu, F.Y.; Lu, J.; Wang, W.L. Oligomerization reactions for precursors to secondary organic aerosol: Comparison between two formation mechanisms for the oligomeric hydroxyalkyl hydroperoxides. *Atmos. Environ.* **2017**, *166*, 1–8. [CrossRef]
62. Kenseth, C.M.; Huang, Y.L.; Zhao, R.; Dalleska, N.F.; Hethcox, C.; Stoltz, B.M.; Seinfeld, J.H. Synergistic O-3 + OH oxidation pathway to extremely low-volatility dimers revealed in beta-pinene secondary organic aerosol. *Proc. Natl. Acad. Sci. USA* **2018**, *115*, 8301–8306. [CrossRef]
63. Chen, L.; Huang, Y.; Xue, Y.G.; Shen, Z.X.; Cao, J.J.; Wang, W.L. Mechanistic and kinetics investigations of oligomer formation from Criegee intermediate reactions with hydroxyalkyl hydroperoxides. *Atmos. Chem. Phys.* **2019**, *19*, 4075–4091. [CrossRef]
64. Zhao, Z.X.; Zhang, W.; Alexander, T.; Zhang, X.; Martin, D.B.C.; Zhang, H.F. Isolating a-Pinene Ozonolysis Pathways Reveals New Insights into Peroxy Radical Chemistry and Secondary Organic Aerosol Formation. *Environ. Sci. Technol.* **2021**, *55*, 6700–6709. [CrossRef] [PubMed]
65. Tomaz, S.; Wang, D.; Zabalegui, N.; Li, D.; Lamkaddam, H.; Bachmeier, F.; Vogel, A.; Monge, M.E.; Perrier, S.; Baltensperger, U.; et al. Structures and reactivity of peroxy radicals and dimeric products revealed by online tandem mass spectrometry. *Nat. Commun.* **2021**, *12*, 300. [CrossRef]
66. Inomata, S. New Particle Formation Promoted by OH Reactions during alpha-Pinene Ozonolysis. *ACS Earth Space Chem.* **2021**, *5*, 1929–1933. [CrossRef]

67. Jia, L.; Xu, Y.F. The role of functional groups in the understanding of secondary organic aerosol formation mechanism from alpha-pinene. *Sci. Total Environ.* **2020**, *738*, 139831. [CrossRef]
68. Roldin, P.; Ehn, M.; Kurten, T.; Olenius, T.; Rissanen, M.P.; Sarnela, N.; Elm, J.; Rantala, P.; Hao, L.Q.; Hyttinen, N.; et al. The role of highly oxygenated organic molecules in the Boreal aerosol-cloud-climate system. *Nat. Commun.* **2019**, *10*, 4370. [CrossRef] [PubMed]
69. Bianchi, F.; Kurten, T.; Riva, M.; Mohr, C.; Rissanen, M.P.; Roldin, P.; Berndt, T.; Crounse, J.D.; Wennberg, P.O.; Mentel, T.F.; et al. Highly Oxygenated Organic Molecules (HOM) from Gas-Phase Autoxidation Involving Peroxy Radicals: A Key Contributor to Atmospheric Aerosol. *Chem. Rev.* **2019**, *119*, 3472–3509. [CrossRef]
70. Frege, C.; Ortega, I.K.; Rissanen, M.P.; Praplan, A.P.; Steiner, G.; Heinritzi, M.; Ahonen, L.; Amorim, A.; Bernhammer, A.K.; Bianchi, F.; et al. Influence of temperature on the molecular composition of ions and charged clusters during pure biogenic nucleation. *Atmos. Chem. Phys.* **2018**, *18*, 65–79. [CrossRef]
71. Crounse, J.D.; Nielsen, L.B.; Jorgensen, S.; Kjaergaard, H.G.; Wennberg, P.O. Autoxidation of Organic Compounds in the Atmosphere. *J. Phys. Chem. Lett.* **2013**, *4*, 3513–3520. [CrossRef]
72. Caravan, R.L.; Vansco, M.F.; Lester, M.I. Open questions on the reactivity of Criegee intermediates. *Commun. Chem.* **2021**, *4*, 44. [CrossRef] [PubMed]
73. Chhantyal-Pun, R.; Rotavera, B.; McGillen, M.R.; Khan, M.A.H.; Eskola, A.J.; Caravan, R.L.; Blacker, L.; Tew, D.P.; Osborn, D.L.; Percival, C.J.; et al. Criegee Intermediate Reactions with Carboxylic Acids: A Potential Source of Secondary Organic Aerosol in the Atmosphere. *ACS Earth Space Chem.* **2018**, *2*, 833–842. [CrossRef]
74. Zhong, J.; Kumar, M.; Zhu, C.Q.; Francisco, J.S.; Zeng, X.C. Surprising Stability of Larger Criegee Intermediates on Aqueous Interfaces. *Angew. Chem. Int. Edit* **2017**, *56*, 7740–7744. [CrossRef]
75. Sakamoto, Y.; Yajima, R.; Inomata, S.; Hirokawa, J. Water vapour effects on secondary organic aerosol formation in isoprene ozonolysis. *Phys. Chem. Chem. Phys.* **2017**, *19*, 3165–3175. [CrossRef]
76. Lin, J.J.M.; Chao, W. Structure-dependent reactivity of Criegee intermediates studied with spectroscopic methods. *Chem. Soc. Rev.* **2017**, *46*, 7483–7497. [CrossRef] [PubMed]
77. Nguyen, T.B.; Tyndall, G.S.; Crounse, J.D.; Teng, A.P.; Bates, K.H.; Schwantes, R.H.; Coggon, M.M.; Zhang, L.; Feiner, P.; Milller, D.O.; et al. Atmospheric fates of Criegee intermediates in the ozonolysis of isoprene. *Phys. Chem. Chem. Phys.* **2016**, *18*, 10241–10254. [CrossRef]
78. Gong, Y.W.; Chen, Z.M. Quantification of the role of stabilized Criegee intermediates in the formation of aerosols in limonene ozonolysis. *Atmos. Chem. Phys.* **2021**, *21*, 813–829. [CrossRef]
79. Sheps, L.; Rotavera, B.; Eskola, A.J.; Osborn, D.L.; Taatjes, C.A.; Au, K.; Shallcross, D.E.; Khan, M.A.H.; Percival, C.J. The reaction of Criegee intermediate CH_2OO with water dimer: Primary products and atmospheric impact. *Phys. Chem. Chem. Phys.* **2017**, *19*, 21970–21979. [CrossRef] [PubMed]
80. Long, B.; Bao, J.L.; Truhlar, D.G. Unimolecular reaction of acetone oxide and its reaction with water in the atmosphere. *Proc. Natl. Acad. Sci. USA* **2018**, *115*, 6135–6140. [CrossRef] [PubMed]
81. Taatjes, C.A. Criegee Intermediates: What Direct Production and Detection Can Teach Us About Reactions of Carbonyl Oxides. *Annu. Rev. Phys. Chem.* **2017**, *68*, 183–207. [CrossRef] [PubMed]
82. Donahue, N.M.; Kroll, J.H.; Pandis, S.N.; Robinson, A.L. A two-dimensional volatility basis set—Part 2: Diagnostics of organic-aerosol evolution. *Atmos. Chem. Phys.* **2012**, *12*, 615–634. [CrossRef]
83. Heinritzi, M.; Dada, L.; Simon, M.; Stolzenburg, D.; Wagner, A.C.; Fischer, L.; Ahonen, L.R.; Amanatidis, S.; Baalbaki, R.; Baccarini, A.; et al. Molecular understanding of the suppression of new-particle formation by isoprene. *Atmos. Chem. Phys.* **2020**, *20*, 11809–11821. [CrossRef]
84. Bonn, B.; Schuster, G.; Moortgat, G.K. Influence of water vapor on the process of new particle formation during monoterpene ozonolysis. *J. Phys. Chem. A* **2002**, *106*, 2869–2881. [CrossRef]
85. Jonsson, A.M.; Hallquist, M.; Ljungstrom, E. Influence of OH scavenger on the water effect on secondary organic aerosol formation from ozonolysis of limonene, Delta(3)-carene, and alpha-pinene. *Environ. Sci. Technol.* **2008**, *42*, 5938–5944. [CrossRef] [PubMed]
86. Kristensen, K.; Jensen, L.N.; Quelever, L.L.J.; Christiansen, S.; Rosati, B.; Elm, J.; Teiwes, R.; Pedersen, H.B.; Glasius, M.; Ehn, M.; et al. The Aarhus Chamber Campaign on Highly Oxygenated Organic Molecules and Aerosols (ACCHA): Particle formation, organic acids, and dimer esters from alpha-pinene ozonolysis at different temperatures. *Atmos. Chem. Phys.* **2020**, *20*, 12549–12567. [CrossRef]